Time-resolved photoelectron angular distributions from nonadiabatically aligned CO_2 molecules with SX-FEL at SACLA

Journal of Physics Communications

PAPER

Time-resolved photoelectron angular distributions from nonadiabatically aligned CO_2 molecules with SX-FEL at SACLA

Shinichirou Minemoto[1], **Hiroyuki Shimada**[2], **Kazma Komatsu**[1], **Wataru Komatsubara**[1], **Takuya Majima**[3], **Soichiro Miyake**[1], **Tomoya Mizuno**[4], **Shigeki Owada**[5], **Hirofumi Sakai**[1], **Tadashi Togashi**[5], **Makina Yabashi**[6], **Piero Decleva**[7], **Mauro Stener**[7], **Shota Tsuru**[2] and **Akira Yagishita**[2,8]

[1] Graduate School of Science, The University of Tokyo, 7-3-1 Hongo, Bunkyo-ku, Tokyo 113-0033 Japan
[2] Institute of Material Structure Science, KEK, 1-1 Oho, Tsukuba, Ibaraki 305-0801 Japan
[3] Quantum Science and Engineering Center, Kyoto University, Uji, Kyoto 611-0011 Japan
[4] Institute of Solid State Physics, The University of Tokyo, 5-1-5 Kashiwanoha, Kashiwa, Chiba 277-8581 Japan
[5] Japan Synchrotron Radiation Research Institute, 1-1-1 Kouto, Sayo-cho, Sayo-gun, Hyogo 679-5198 Japan
[6] RIKEN SPring-8 Center, 1-1-1 Kouto, Sayo-cho, Sayo-gun, Hyogo 679-5148 Japan
[7] Dipartimento di Scienze Chimiche, Università di Trieste, Via L. Giorgieri I, I-34127 Trieste, Italy
[8] Author to whom any correspondence should be addressed.

E-mail: akira.yagishita@kek.jp

Keywords: photoelectron spectroscopy, aligned molecules, photoelectron angular distribution, free electron laser

OPEN ACCESS

RECEIVED
24 September 2018

REVISED
29 September 2018

ACCEPTED FOR PUBLICATION
2 November 2018

PUBLISHED
14 November 2018

Abstract

We performed time-resolved photoelectron spectroscopy of valence orbitals of aligned CO_2 molecules using the femtosecond soft x-ray free-electron laser and the synchronized near-infrared laser. By properly ordering the individual single-shot ion images, we successfully obtained the photoelectron angular distributions (PADs) of the CO_2 molecules aligned in the laboratory frame (LF). The simulations using the dipole matrix elements due to the time dependent density functional theory calculations well reproduce the experimental PADs by considering the axis distributions of the molecules. The simulations further suggest that, when the degrees of alignment can be increased up to $\langle \cos^2\theta \rangle > 0.8$, the molecular geometries during photochemical reactions can be extracted from the measured LFPADs once the accurate matrix elements are given by the calculations.

1. Introduction

Recent developments of x-ray free electron lasers (XFELs) [1–4] and table-top laser sources [5] are bringing off ultrafast imaging of molecules with femtosecond temporal and sub-Ångstrom spatial resolutions [6–9]. The first imaging of atomic motions during photochemical processes has been achieved by the ultrafast electron diffraction (UED) [10–12] and the ultrafast x-ray diffraction (UXD) [13–16]. Other imaging techniques such as the Coulomb explosion imaging (CEI) [17–20], the laser-induced electron diffraction (LIED) [21–23], and the ultrafast x-ray photoelectron diffraction (UXPD) [24–36] are also in progress. Among them, characteristic features of the XPD are element-specific and chemical-state-specific. More importantly, the x-ray photoionization cross sections are of four to six orders of magnitude larger than those for x-ray scattering [37]. From these reasons, the XPD is widely used for short-range surface structure analysis [38–40].

However, the UXPD for gas-phase molecules is only possible by fixing the molecules in space [41]. For instance, a spatiotemporal control of the axis distribution (alignment) for the molecular ensemble in the laboratory frame (LF) can be obtainable due to a rotational wave packet created with femtosecond IR laser pulses. Hence, at any given delay time between the IR pump and ionizing probe laser pulses, a set of different molecular alignment and polarization geometry is probed. That is, by preparing an aligned sample of molecules, the axis distributions and photoelectron angular distributions (PADs) from the relevant molecular ensemble can be observed in the LF [42–45]. Up to now, such ultrafast time-resolved LFPADs have been intensively studied to gain insight into intramolecular dynamics [46–52]. In contrast to this, ultrafast molecular frame PADs (MFPADs) are now in progress, so that the present status of the UXPD is limited [29–34]. Namely, the ultrafast

MFPADs are necessarily demanding to determine ultrafast atomic motions during photochemical processes. In other words, the ultrafast processes such as dissociation, isomerization and intersystem crossing are best understood by MFPADs.

In the above mentioned context, prior to the final goal of the UXPD, here we present the time-resolved PADs from an aligned CO_2 molecular ensemble with the femtosecond soft x-ray (SX) pulses from SACLA SX-FEL [53]. The aligned molecular ensemble was prepared using the SACLA in-house Ti:sapphire NIR laser [54], and then evolves under field-free conditions. On one hand, the degree of alignment for the CO_2 molecular ensemble was determined by one of the facing velocity map imaging spectrometers (VMIs) [32, 34, 55], which recorded the momentum distribution of CO^+ fragment ions resulting from Coulomb explosion of the doubly-charged CO_2^{2+} ions produced through double ionization by SX-FEL. On the other hand, using the other VMI, the time-resolved valence orbital PADs from the aligned molecular ensemble by SX-FEL was observed in the LF. Because the evolution of the prepared molecular ensemble is independent of ionization by the probe femtosecond SX pulses, one can consider such time-resolved PADs to be those from the partially aligned molecular ensemble, the degree of which was simultaneously determined by our facing VMIs. In the end, we will make the differences between the LFPADs for partially aligned molecules and the randomly aligned MFPAD clear, based on numerical simulations, since the interpretations of such PADs are often confused in the literatures [31, 49, 51].

2. Experiment

The experiments were performed at the SX beamline BL1 at SACLA [53]. The SX-FEL was operated at the wavelength of 22.4 nm (55.4 eV) and the bandwidth of ~2% (~1 eV). The duration of the SX-FEL pulses, τ_X, was estimated as ~100 fs (FWHM) and the pulse energy was ~50 μJ with a diameter of ~10 μm. For the pump laser pulses, we used the optical laser system synchronized to SX-FEL at SACLA [54]. The Ti:sapphire NIR laser was operated at the central wavelength of 793 nm (1.56 eV) and the bandwidth of ~30 nm. The NIR laser pulse duration, τ_L, measured by a single-shot autocorrelator was 300 fs (FWHM), which was slightly stretched from the Fourier-limited pulse to reduce the effects of timing jitter between the NIR and SX-FEL pulses. The NIR pulse energy was ~5 mJ; the peak intensities on the order of 10^{14} W cm^{-2} could be reached at the focus of ~100 μm. The NIR laser beam was combined with the SX-FEL beam by a holey mirror in a vacuum chamber almost collinearly, and the spatial overlap between the two beams was monitored by a Ce:YAG screen inserted in the center of the facing VMI spectrometers, see [32, 34] for details. The delay time t between the NIR and SX-FEL pulses was controlled by a translational stage inserted in the NIR beam path. Firstly, the delay time t was roughly scanned with an interval of 0.67 ps between $t = -2$ ps and 47 ps. From this, overall behavior of the degree of alignment, $\langle \cos^2\theta \rangle$, during the first rotational period, $T_{rot} = 42.7$ ps, was examined, including the timing of the rapid modurations around $t = 0$ and T_{rot} and the degrees of so-called permanent alignment (the DC level due to higher J states [56]). Next, the delay time t was finely scanned with an interval of 0.2 ps at around delay times when $\langle \cos^2\theta \rangle$ exhibits rapid modulations; near the pump pulse irradiation (from $t = -1.6 to 2.0$ ps), around the half revival (from $t = 18.7$ to 24.6 ps), and around the full revival (from $t = 40.8$ to 46.8 ps). The pulsed molecular beam was crossed by the collinear laser beams. Then, the electrons produced in the interaction region were drawn into the lower VMI, while the ions were drawn into the upper VMI: the former recorded two-dimensional (2D) photoelectron momentum images, and the latter recorded 2D ion momentum images. Here, for the ion detection, we applied a pulsed high voltage of −2 kV to the microchannel plate at the flight time corresponding to a specific mass-to-charge ratio. By this gating procedure, we measured only the desired CO^+ fragment ions, which best represent the angular distributions of the molecular axis.

On one hand, both the SX-FEL and the synchronized NIR laser were operated at a repetition rate of 30 Hz. On the other hand, the pulsed valve for the molecular beam was operated at a 15 Hz repetition rate. Thus, the 2D images (signal + background) with and those (background) without the sample molecules were alternately measured, and then the 2D images without both the noise from the residual gas and from the scattered XUV were obtained by subtracting the background from the (signal + background) 2D images. The 2D data set consists of 2,500 images at each delay time.

3. Results and discussions

3.1. Alignment of CO_2 induced by NIR laser

In order to obtain the alignment states of the molecular axis, we analyzed the concentric parts in the CO^+ fragment ion images, which correspond to the Coulomb explosion channel of $CO^+ + O^+$ from the doubly ionized molecular ions CO_2^{2+}. Then, we introduced the orientation distribution function $F(\theta, t)$ [57], which is defined by

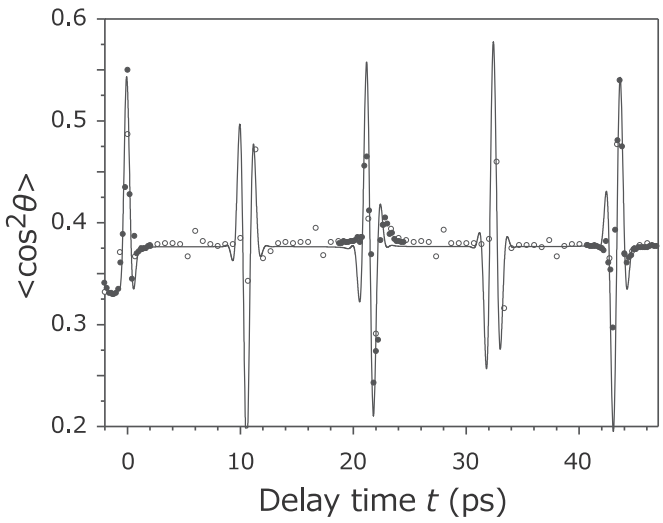

Figure 1. Evolution of the degree of alignment $\langle \cos^2\theta \rangle$ as a function of the delay time t between the alignment NIR and SX-FEL probe pulses. Open and solid circles; experimental data for the rough and the fine scans, respectively, evaluated from the CO^+ fragment ions. Solid line; the theoretical calculation under the rotational temperature of 6 K and the peak intensity of the NIR laser of 5×10^{13} W cm^{-2}.

$$F(\theta, t) = \frac{I(\theta, t)}{I_{\mathrm{ran}}(\theta)}, \tag{1}$$

where $I(\theta, t)$ is the CO^+ ion signal intensities at the delay time t, and I_{ran} the intensities at $t = -0.4$ ps, which corresponds to the random orientation. The angle θ is the ejection angle of the CO^+ fragment ion relative to the polarization vector of the NIR laser pulse. The function $F(\theta, t)$ is normalized to $\int_{-\pi}^{\pi} F(\theta, t)|\sin\theta| d\theta = 1$, so that the time-dependent degree of alignment $\langle \cos^2\theta \rangle(t)$ can be described by

$$\langle \cos^2\theta \rangle(t) = \int_{-\pi}^{\pi} F(\theta, t) \cos^2\theta |\sin\theta| d\theta. \tag{2}$$

Since the FEL pulses are generated by the self-amplified spontaneous emission (SASE) process [58], their intensities and temporal and spectral shapes vary significantly from shot to shot, and moreover the FEL pulses have a finite timing jitter on the order of ~1 ps with the synchronized optical pulses [55]. Thus, in our experiment, the degrees of alignment were much decreased due to the inevitable timing jitter between the SX-FEL and NIR pulses, i.e., the fluctuation of t [55]. To remove the degradation of the alignment due to the timing jitter, we tried to rearrange the single-shot ion images by referring to the theoretical values for the degree of alignment: Firstly, the degrees of alignment were calculated by solving the time-dependent Schrödinger equation according to [59]. The calculated results under the rotational temperature of 6 K and the peak intensity of the NIR laser of 5×10^{13} W cm^{-2} are shown in figure 1. Among the parameters investigated, the results with these values best reproduce the maximum $\langle \cos^2\theta \rangle(t)$ of 0.540 at around T_{rot} and the permanent alignment with $\langle \cos^2\theta \rangle(t) = 0.377$ simultaneously, both of which are experimental observations. Secondly, at $\sim T_{\mathrm{rot}}/2$ and $\sim T_{\mathrm{rot}}$, the delay time t for each ion image was ordered within 0.7 ps by comparing the degrees of alignment determined from the image with the calculated ones. Thus, the 2,500 images for a single nominal delay time were distributed to seven different delay times. Finally, we obtained the reasonably ordered results of the time evolution of $\langle \cos^2\theta \rangle(t)$, which is depicted in figure 1. By this cumbersome procedure, we got rid of the timing jitter effects on the time evolution of the alignment degrees partially.

Just after the irradiation of the NIR pump pulse, the rotational wave packet is created, showing maximum $\langle \cos^2\theta \rangle$ of 0.540 at $t = 0.4$ ps. Following the dephasing, the rotational wave packet shows a permanent alignment with $\langle \cos^2\theta \rangle = 0.377$. The degree of alignment $\langle \cos^2\theta \rangle$ modulates with an interval of 10.6 ps, which corresponds to $T_{\mathrm{rot}}/4$, and the rotational wave packet rephases at 22.0 ps ($\sim T_{\mathrm{rot}}/2$) and 43.6 ps ($\sim T_{\mathrm{rot}}$) showing the minimum $\langle \cos^2\theta \rangle = 0.255$ and the maximum $\langle \cos^2\theta \rangle = 0.540$, respectively. A slight mismatch between the experimental and theoretical results may be due to the incomplete arrangement of the delay time and to the uneven detection efficiencies when the desired ions were gated. Since the duration of the gating pulse was as short as the width of the flight time of the fragment ions, the detection efficiencies might depend on the azimuth angles of ion ejection, by which $\langle \cos^2\theta \rangle$ might be slightly underestimated.

To evaluate the degree of alignment $\langle \cos^2\theta \rangle$ by equation (2) in the above mentioned procedure, we derive the time-dependent orientation distribution function $F(\theta, t)$ from the CO^+ fragment ion images. Such functions are shown in figure 2. Taking the molecular symmetry of the CO_2 into account, this orientation

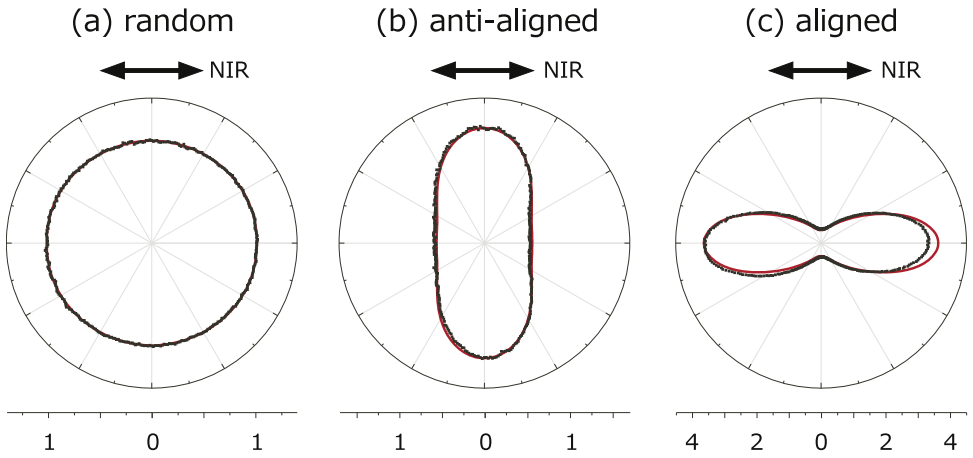

Figure 2. The orientation distribution functions $F(\theta, t)$ of equation (1). (a) $t = -0.4$ ps, $\langle \cos^2\theta \rangle = 0.333$, (b) $t = 22.0$ ps, $\langle \cos^2\theta \rangle = 0.255$, and (c) $t = 43.6$ ps, $\langle \cos^2\theta \rangle = 0.540$. Dots; experimental results, and solid lines; fitted results of equation (3). Polarization vector of the NIR laser is shown by the double-headed arrows. The distribution functions are used for the theoretical simulations of equation (4). The statistical errors of the experimental results are $\pm 0.5\%$.

Table 1. The coefficients $a_K(t)$ of the Legendre polynominals $P_K(\theta)$ in equation (3).

t	$\langle \cos^2\theta \rangle$	a_0	a_2	a_4	a_6	a_8	a_{10}	a_{12}	a_{14}
−0.4 ps	0.333	1.000	0.001						
22.0 ps	0.255	0.986	−0.583	0.159	−0.002	−0.008			
43.6 ps	0.540	0.999	1.549	0.674	0.181	0.074			
11.2 ps[a]	0.839	0.997	3.372	5.816	5.555	7.810	7.605	9.901	9.940

[a] The delay time at which the theoretical calculation gives the highest value of $\langle \cos^2\theta \rangle$ under the condition of the rotational temperature of 6 K and the peak intensity of 2×10^{14} W cm^{-2}.

distribution function $F(\theta, t)$ can be expanded by the Legendre polynominals $P_K(\cos\theta)$ of even integers of K;

$$F(\theta, t) = \sum_K a_K(t) P_K(\cos\theta). \quad (3)$$

Thus, to derive the coefficients $a_K(t)$, equation (3) was fitted to the experimental results at $t = -0.4$, $22.0 (\sim T_{\rm rot}/2)$, and 43.6 ps $(\sim T_{\rm rot})$. The fitted curves are shown in figure 2 together with the experimental data. The obtained values of $a_K(t)$ are summarized in table 1 with the corresponding values of the degrees of alignment.

3.2. Photoelectron angular distributions from aligned CO_2

The 2D photoelectron images by 55.4-eV photons of the SX-FEL, which are the counterpart of the properly ordered ion images in the previous section, are Abel inverted by the pBASEX procedure [60] to obtain the 2D cut of the 3D photoelectron momentum distribution. Figure 3 displays the inverted Abel image of photoelectrons from the CO_2 molecules aligned along the polarization vector of the NIR laser pulse. In our experimental condition, the polarization vectors of both the NIR pump and the SX-FEL probe pulses are parallel to each other. The lower panel shows the corresponding photoelectron spectrum, which was obtained by the integration over all the emission angles of the photoelectrons. The peak labeled by X at the kinetic energy of 42eV, which corresponds to the outermost ring in the Abel inverted image, can be attributed to the ionization of $1\pi_g$ level of the CO_2, resulting in the X state of the CO_2^+ ions [61]. The peak labeled by A, B, and C at 38eV is the ionization of $1\pi_u$, $3\sigma_u$, and $4\sigma_g$ levels, resulting in the lower excited states, A, B, and C of the CO_2^+. The energy resolution of our VMI, $\Delta E/E$ of ~5%, can distinguish the X state from the other excited states, while these excited states are merged to a single peak. The inner valence photoelectrons are observed at 18, 25, and 30 eV, which are obscured by the tail of back scattering electrons from the microchannel plate for the ion detection[91]. The photoelectron

[9] Due to the voltage settings of the VMIs, some of electrons produced at the surface of the microchannel plate for the ion detection are accelerated toward that for photoelectron detection. They are detected as signals at later flight times and with broad and smaller kinetic energies than proper photoelectron signals.

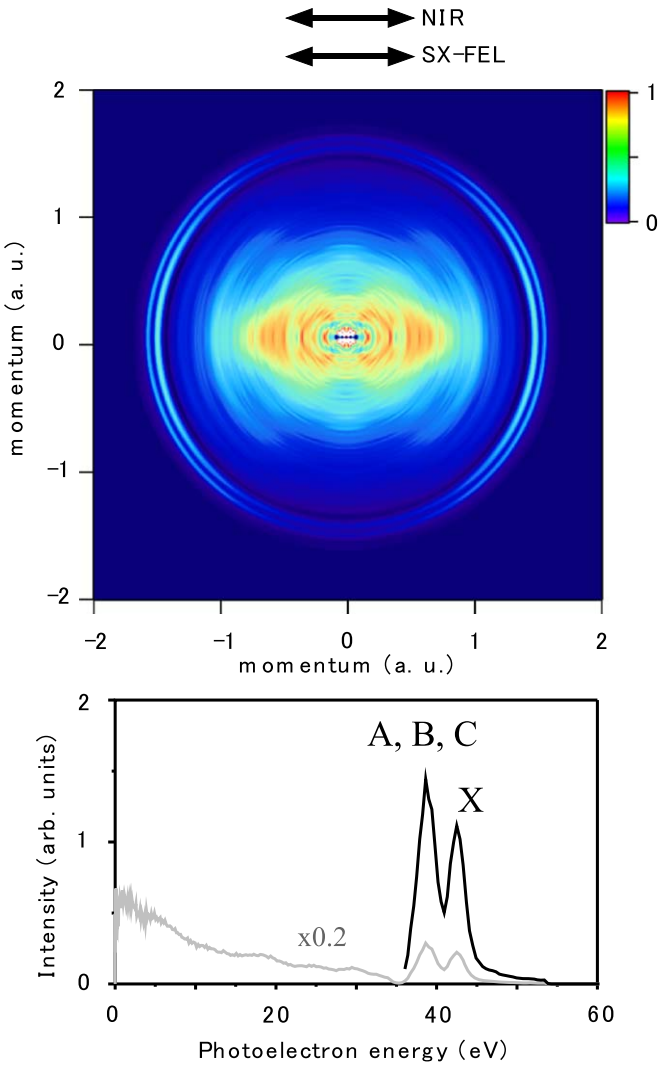

Figure 3. Abel inverted image of photoelectrons from CO_2 molecules at $t = 43.6$ ps (upper) and the corresponding angle-integrated photoelectron energy spectrum (lower). Polarization vectors of the NIR and SX-FEL are parallel to each other as shown by the double-headed arrows. The peak labeled A at 42 eV are attributed to the ionization of $1\pi_g$ level and those labeled C, B, and C at 38 eV to the $1\pi_u$, $3\sigma_u$, and $4\sigma_g$ levels. The statistical errors are less than $\pm 1\%$.

spectra integrated over all the angles, i.e., the photoionization cross sections for each level, were independent of the delay time t, in other words, the degree of alignment, although they are not shown here, as can be expected.

In what follows we consider the photoelectron angular distributions (PADs) from the valence levels of the aligned CO_2 molecules. The time-dependent PADs from the $1\pi_g$ level of the CO_2 are demonstrated as the polar plots in figure 4; (a) $t = -0.4$ ps (randomly aligned), (b) $t = 22.0$ ps (aligned perpendicular to the polarization vector), and (c) $t = 43.6$ ps (aligned along the polarization vector). Such laboratory frame PADs (LFPADs) from the aligned molecular ensemble are described by the sum of the molecular frame PADs (MFPADs) [62] weighted by the orientation distribution function of equation (3) [63]. Taking both the polarization vector of the SX-FEL along the LF z-axis and the symmetry of the CO_2 molecules into account, the time-dependent LFPAD can be expressed by [63]

$$I(\theta_e, t) \propto \sum_{L,L_\gamma,K,M} (10,\ 10|L_\gamma 0) A_{LM}^{L_\gamma} (-1)^M (L - M,\ L_\gamma M|K0)(L0,\ L_\gamma 0|K0) \times \frac{\sqrt{2L+1}}{(2K+1)} a_K(t) P_L(\cos\theta_e) \tag{4}$$

where the dynamical parameter $A_{LM}^{L_\gamma}$ is described by the dipole matrix elements for photoionization [64], L the vector sum of the angular momenta of photoelectron partial waves in the MF, L_γ (=0 and 2) the vector sum of photon angular momentum, and θ_e the angle between the photoelectron momentum and the LF z-axis. Since L_γ and K are even integers, even integers of L are allowed by the non-zero conditions of the Clebsch–Gordan coefficients, $(L0,\ L_\gamma 0|K0) \neq 0$, in equation (4), and also the maximum integer of L is given by the condition.

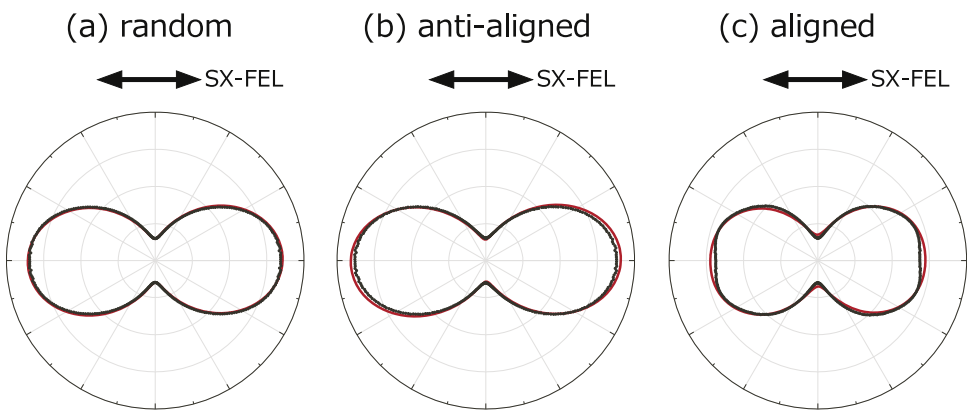

Figure 4. LFPADs for the $1\pi_g$ level of the CO_2. (a) $t = -0.4$ ps, $\langle \cos^2\theta \rangle = 0.333$, (b) $t = 22.0$ ps, $\langle \cos^2\theta \rangle = 0.255$, and (c) $t = 43.6$ ps, $\langle \cos^2\theta \rangle = 0.540$. Dots; experimental results, and solid lines; theoretical simulation results. Each LFPAD is normalized so that its volume integral becomes unity. Polarization vector of the SX-FEL is shown by the double-headed arrows. The statistical errors of the experimental results are less than $\pm 1\%$. The LFPAD in (c) shows considerable change from those in (a) and (b), which is reasonably reproduced by the simulation.

Using the experimentally determined $a_K(t)$ values in equation (3) and the dipole matrix elements for photoionization of the $1\pi_g$ level calculated with the time-dependent density functional theory (TDDFT) [65], we have simulated the time-dependent LFPADs. The simulation results are shown in figure 4 to compare with the corresponding experimental data. In figure 4(a), the experimental LFPAD is perfectly reproduced by the simulation. It should be noted that the simulated LFPAD for the randomly aligned molecules in figure 4(a) is consistent with the LFPAD for the asymmetry parameter $\beta = 1.26$, which was calculated with the TDDFT. In figure 4(b), both the experimental and simulated LFPAD, for the molecules aligned perpendicular to the polarization vector, are slightly changed from that for the randomly aligned molecules in figure 4(a). In figure 4(c), one can see considerable change of the LFPAD, for the molecules aligned parallel to the polarization vector, from those in figures 4(a) and (b). This change is reasonably reproduced by the simulated LFPAD according to equation (4), which is the average of the MFPAD over the molecular orientation, as can be seen in the figure.

The LFPADs for the sum of the $1\pi_u$, $3\sigma_u$, and $4\sigma_g$ levels didn't exhibit the alignment-dependent nature, i.e., time-dependent nature, although they are not shown here.

4. Summary and outlook

Using quantum mechanical nature, i.e., revival of the rotational wave packets, which were induced by the femtosecond NIR laser, we have measured the time-dependent LFPADs from the partially aligned CO_2 molecules under the field-free condition. The time dependent LFPADs have been well reproduced by the TDDFT calculations considering the time-dependent degree of alignment, in other words, molecular axis distributions. In this context, higher degree of alignment is most desirable in developing the UXPD.

To get a feeling on the alignment effect on the LFPAD, we simulated the LFPADs for the $1\pi_g$ level of the CO_2 at the photon energy of 55.4 eV, under the condition of $\langle \cos^2\theta \rangle = 0.84$ (see the last line in table 1). This degree of alignment was calculated under the extreme experimental condition of the rotational temperature of 6 K and the peak intensity of the NIR laser of 2×10^{14} W cm^{-2}. The simulation results are shown in figure 5. As can be seen from the figure, under the present experimental condition of $\langle \cos^2\theta \rangle = 0.54$, the characteristic feature of the MFPAD in figure 5(c) consisting of lobes and nodes are fully smeared out by the convolution of it with the molecular axis distributions. In contrast to this, under the promising condition of $\langle \cos^2\theta \rangle = 0.84$, every lobe and node of the MFPAD is observed in the LFPAD. From this, we can say that when one can measure the LFPAD, for example, for the degree of alignment $\langle \cos^2\theta \rangle > 0.8$, one can determine the matrix elements of the photoionization by the analyses of such experimental LFPAD, on the analogy of our previous works on the complete photoionization experiments, which derives the matrix elements from the MFPAD measured from the photoelectron-fragment-ion coincidence experiments [66]. Conversely, one can derive the unknown molecular geometry from the experimental MFPAD or LFPAD measured with the high degree of alignment, when the theoretical calculations give accurate matrix elements of the photoionization for a given molecular geometry. In this context, the geometrical change of laser-aligned molecules caused by another femtosecond optical laser can be probed by the SX-FEL. This is our scenario of the UXPD: we trigger the photochemical reaction by an optical

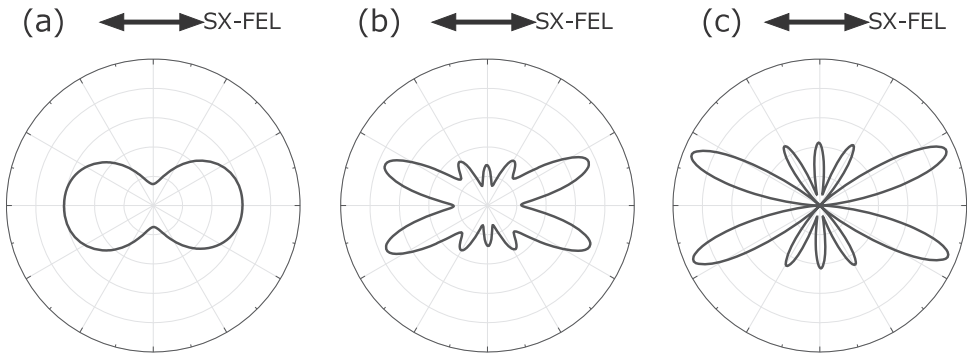

Figure 5. Simulation of LFPADs (a), (b) and MFPAD (c) for the $1\pi_g$ level of CO_2 at the photon energy of 55.4 eV. (a); $\langle \cos^2\theta \rangle = 0.540$, same as figure 4(c), (b); $\langle \cos^2\theta \rangle = 0.839$, (c); perfect alignment. Each PAD is normalized so that its volume integral becomes unity. Polarization vector of the SX-FEL is shown by the double-headed arrows. In (c), the molecular axis is parallel to the polarization vector. The lobes and nodes of (c) are fully smeared out in (a) while they are clearly observed in (b).

laser and determine ultrafast atomic motions by SX-FEL during dissociation, isomerization and intersystem crossing [25, 35, 36].

In the end, we can say that we stepped towards the final goal of the UXPD by the success of the time-resolved LFPAD measurement in the present work.

Acknowledgments

The authors appreciate fruitful discussions with J. Itatani (The University of Tokyo). They thank the operation and engineering staff members of SACLA for their support in performing the XFEL experiments, which were conducted at the BL1 of SACLA with the approval of the Japan Synchrotron Radiation Research Institute (JASRI) (Proposal No. 2017B8011). They acknowledge the computer time in CINECA through the IseC_UTREP grant. This work is financially supported from JSPS KAKENHI (Nr. 16H02132, Nr. 16K05496, and Nr. 17H05214). K K and W K are financially supported by Advanced Leading Graduate Course for Photon Science (ALPS) of MEXT.

ORCID iDs

Shinichirou Minemoto https://orcid.org/0000-0001-5868-823X
Hiroyuki Shimada https://orcid.org/0000-0003-0207-2238
Takuya Majima https://orcid.org/0000-0003-2804-1915
Shota Tsuru https://orcid.org/0000-0003-0014-7873

References

[1] Emma P *et al* 2010 *Nat. Photon.* **4** 641
[2] Ishikawa T *et al* 2012 *Nat. Photon.* **6** 540
[3] Margaritondo G 2017 *Riv. Nuovo Cimento* **40** 411–71
[4] Helml W *et al* 2017 *Appl. Sci.* **7** 915
[5] Calegari F *et al* 2016 *J. Phys. B: At., Mol. Opt. Phys.* **49** 062001
[6] Elsaesser T E and Woerner M 2014 *J. Chem. Phys.* **140** 020901
[7] Xu J, Blaga C I, Agostini P and DiMauro L F 2016 *J. Phys. B: At., Mol. Opt. Phys.* **49** 112001
[8] Miller R J D 2016 *Faraday Discuss.* **194** 777
[9] Elsaesser T 2017 *Chem. Rev.* **117** 10621
[10] Yang J *et al* 2016 *Phys. Rev. Lett.* **117** 153002
[11] Vecchione T *et al* 2017 *Rev. Sci. Instrum.* **88** 033702
[12] Zandi O, Wilkin K J, Xiong Y and Centurion M 2017 *Struct. Dyn.* **4** 044022
[13] Glownia J M *et al* 2016 *Phys. Rev. Lett.* **117** 153003
[14] Kirrander A and Weber P M 2017 *Appl. Sci.* **7** 534
[15] Kowalewski M, Bennett K and Mukamel S 2017 *Struct. Dyn.* **4** 054101
[16] Chergui M and Collet E 2017 *Chem. Rev.* **117** 11025
[17] Légaré F *et al* 2006 *J. Phys. B: At., Mol. Opt. Phys.* **39** S503
[18] Cornaggia C 2009 *Laser Phys.* **19** 1660
[19] Karimi R, Liu W-K and Sanderson J 2016 Femtosecond laser-induced Coulomb explosion imaging (*Advances in Multi-Photon Processes and Spectroscopy* vol 23) ed S H Lin, A A Villaeys and Y Fujimura (Singapore: World Scientific)
[20] Burt M *et al* 2017 *Phys. Rev.* A **96** 043415

[21] Ito Y et al 2016 Struct. Dyn. 3 034303
[22] Wolter B et al 2016 Science 354 308
[23] Morimoto Y, Kanya R and Yamanouchi K 2017 Laser-assisted electron scattering and diffraction for ultrafast imaging of atoms and molecules Progress in Photon Science ed K Yamanouchi (Berlin: Springer)
[24] Krasniqi F et al 2010 Phys. Rev. A 81 033411
[25] Kazama M et al 2013 Phys. Rev. A 87 063417
[26] Sun S X-L, Kaduwela A P, Gray A X and Fadley C S 2014 Phys. Rev. A 89 053415
[27] Wang X et al 2016 Sci. Rep. 6 23655
[28] Nguyen N-T, Lucchese R R, Lin C D and Le A-T 2016 Phys. Rev. A 93 063419
[29] Boll R et al 2013 Phys. Rev. A 88 061402(R)
[30] Rolles D et al 2014 J. Phys. B: At., Mol. Opt. Phys. 47 124035
[31] Boll R et al 2014 Faraday Discuss. 171 57
[32] Nakajima K et al 2015 Sci. Rep. 5 14065
[33] Yagishita A 2015 J. Electron Spectrosc. Relat. Phenom. 200 247
[34] Minemoto S et al 2016 Sci. Rep. 6 38654
[35] Tsuru S, Sako T, Fujikawa T and Yagishita A 2017 Phys. Rev. A 95 043404
[36] Tsuru S et al 2018 J. Chem. Phys. 148 124101
[37] Stout G H and Jensen L H 1989 X-Ray Structure Determination: A Practical Guide 2nd edn (New York: Wiley)
[38] Berman H M et al 2002 Acta Crystallogr., Sect. D: Biol. Crystallogr. 58 899
[39] Rhodes G 2006 Crystallography Made Crystal Clear: A Guide for Users of Macromolecular Models 3rd edn (San Diego, CA: Academic)
[40] Fadley C S 2010 J. Electron Spectrosc. Relat. Phenom. 178-179 2
[41] Filsinger F et al 2012 Phys. Chem. Chem. Phys. 14 13370–7
[42] Johnson P et al 2009 J. Phys. B: At. Mol. Opt. Phys. 42 134017
[43] Kelkensberg F et al 2011 Phys, Rev. A 84 051404(R)
[44] Marceau C et al 2017 Phys. Rev. Lett. 119 083401
[45] Reid K L et al 1999 J. Chem. Phys. 111 1438
[46] Tsubouchi M et al 2001 Phys. Rev. Lett. 86 4500
[47] Suzuki T 2006 Annu. Rev. Phys. Chem. 57 555
[48] Kumarappan V et al 2008 Phys. Rev. Lett. 100 093006
[49] Bisgaard C Z et al 2009 Science 323 1464
[50] Holmegaard L et al 2010 Nat. Phys. 6 428
[51] Maurer J et al 2012 Phys. Rev. Lett. 109 123001
[52] Rouzée A et al 2012 J. Phys. B: At. Mol. Opt. Phys. 45 074016
[53] Owada S et al 2018 J. Synchroton Rad. 25 282
[54] Owada S et al 2018 J. Synchrotron Rad. 25 68
[55] Minemoto S et al 2018 J. Phys. B: At. Mol. Opt. Phys. 51 075601
[56] Søndergaard A A, Shepperson B and Stapelfeldt H 2017 J. Chem. Phys. 147 013905
[57] Minemoto S and Sakai H 2011 J. Chem. Phys. 134 214305
[58] Saldin E L, Schneidmiller E A and Yurkov M V 2000 The Physics of Free Electron Lasers (Berlin: Springer)
[59] Ortigoso J, Rodriguez M, Gupta M and Friedrich B 1999 J. Chem. Phys. 110 3870
[60] Garcia G A, Nahon L and Powis I 2004 Rev. Sci. Instrum. 75 4989
[61] Katsumata S, Achiba Y and Kimura K 1979 J. Electron Spectrosc. Relat. Phenom. 17 229
[62] Dill D et al 1978 Phys. Rev. Lett. 41 1230
[63] See for example Underwood J G and Reid K L 2000 J. Chem. Phys. 113 1067
[64] Motoki S et al 2000 J. Phys. B: At. Mol. Opt. Phys. 33 4193
Yagishita A et al 2005 J. Electron Spectrosc. Relat. Phenom. 142 295
Adachi J et al 2007 J. Phys. B: At. Mol. Opt. Phys. 40 29
[65] Stener M 2005 J. Chem. Phys. 122 234301
[66] Motoki S et al 2002 Phys. Rev. Let. 88 063003
Motoki S et al 2002 J. Phys. B: At. Mol. Opt. Phys. 35 3801
Teramoto T et al 2007 J. Phys. B: At. Mol. Opt. Phys. 40 F241
Teramoto T et al 2007 J. Phys. B: At. Mol. Opt. Phys. 40 4033